

A KELT-*TESS* Eclipsing Binary in a Young, Triple System Associated with the Local “Stellar String” Theia 301

JONI-MARIE C. CUNNINGHAM,¹ DAX L. FELIZ,¹ DON M. DIXON,¹ JOSHUA PEPPER,² KEIVAN G. STASSUN,¹
ROBERT J. SIVERD,¹ GEORGE ZHOU,³ DANIEL BAYLISS,³ THIAM-GUAN TAN,⁴ PHILLIP CARGILE,¹ DAVID JAMES,⁵
RUDOLF B. KUHN,^{6,7} AND MARINA KOUNKEL⁸

¹*Vanderbilt University, Department of Physics & Astronomy, 6301 Stevenson Center Ln., Nashville, TN 37235, USA*

²*Department of Physics, Lehigh University, Bethlehem, PA 18015, USA*

³*Observatoire de Genève*

⁴*Perth Exoplanet Survey Telescope*

⁵*Cerro Tololo Inter-American Observatory, Colina El Pino, S/N, La Serena, Chile*

⁶*South African Astronomical Observatory, P.O. Box 9, Observatory 7935, Cape Town, South Africa*

⁷*Southern African Large Telescope, P.O. Box 9, Observatory 7935, Cape Town, South Africa*

⁸*Western Washington University*

Abstract

HD 54236 is a nearby, wide common-proper-motion visual pair that has been previously identified as likely being very young by virtue of strong X-ray emission and lithium absorption. Here we report the discovery that the brighter member of the wide pair, HD 54236A, is itself an eclipsing binary (EB), comprising two near-equal solar-mass stars on a 2.4-d orbit. It represents a potentially valuable opportunity to expand the number of benchmark-grade EBs at young stellar ages. Using new observations of Ca II H&K emission and lithium absorption in the wide K-dwarf companion, HD 54236B, we obtain a robust age estimate of 225 ± 50 Myr for the system. This age estimate and *Gaia* proper motions show HD 54236 is associated with Theia 301, a newly discovered local “stellar string”, which itself may be related to the AB Dor moving group through shared stellar members. Applying this age estimate to AB Dor itself alleviates reported tension between observation and theory that arises for the luminosity of AB Dor C when younger age estimates are used.

Keywords: stars: low-mass — stars: eclipsing binaries — stars: fundamental parameters — stars: stellar associations

1. INTRODUCTION

Eclipsing binary (EB) stars are foundational to stellar astrophysics by virtue of providing all of the fundamental physical properties of stars to high accuracy, with which to test and benchmark theoretical stellar evolution models, and to probe the ages of interesting Galactic populations. In a review of the field, Torres et al. (2012) identified approximately 100 EBs whose parameters have been determined with sufficient accuracy to serve as stringent model benchmarks. Only one of these benchmark-grade EBs includes stars still in the pre-main-sequence (PMS) phase of evolution (V1174 Ori; Stassun et al. 2004). In addition, only about 25 of these EBs have measured metallicities, and an even smaller number have independent age constraints (as provided by, e.g., membership in clusters or moving groups), limiting the ability of even these benchmark-grade EBs to serve as the most stringent tests of stellar models. Additional benchmarks for early stellar evolution are critical in building our understanding of stellar formation.

A number of ground and space based exoplanet transit surveys are operating that find EBs in large numbers, either as unintentional false positives or as intentional targets. The KELT survey (Pepper et al. 2007, 2012), has so far identified four bright transiting exoplanets (Siverd et al. 2012; Beatty et al. 2012; Pepper et al. 2012; Collins et al. 2014), in conjunction with a very large number of EBs (e.g. Pepper et al. 2008).

In the course of commissioning the KELT-South telescope we identified the bright, X-ray source HD 54236A as an EB. It is listed in the SIMBAD database as a PMS star and listed in the SACY catalog as possessing Li in its spectrum, a diagnostic of stellar youth. It also possesses a wide common-proper-motion (CPM) companion, HD 54236B, which in turn provides the opportunity for independent checks on key parameters such as system age. Most recently, the

Transiting Exoplanet Survey Satellite (*TESS*) observed the HD 54236 system (HD 54236A has TIC ID 238162238 in the TESS Input Catalog; Stassun et al. 2019).

At the same time, the advent of *Gaia* has revolutionized our understanding of stellar multiples (e.g., Oelkers & Stassun 2018), stellar associations (e.g., Oh et al. 2017), and the 3D structure of the solar neighborhood (e.g., Kounkel & Covey 2019). Indeed, very recent investigations of the full phase-space structure of stars in the solar neighborhood reveal previously unrecognized “stellar strings”, long filamentary groups of young stars that appear to encode the large spiral-arm structures from which they formed (Kounkel et al. 2020). Thus, HD 54236 represents a valuable opportunity to expand the number of known benchmark-grade EBs at young stellar ages, and to test recent suggestions of young “stellar strings” in the solar neighborhood.

In §2 we describe the overall context of the HD 54236 system, including the presence of HD 54236B as a known, wide CPM tertiary. In §3 we present the photometric observations and the spectroscopic observations obtained for the system used to identify HD 54236A as a previously unknown EB, and to determine the basic physical properties of the stellar components. In §4 we present the results of our analysis, including orbital solutions, light curve extracted stellar parameters including temperature and radius estimates for both components in the EB, SED modeling and resultant measurement of the stellar masses, and determination of the system age through consideration of the lithium abundances and the Ca II H&K activity. Finally, in §5 we consider the membership of HD 54236 in relation to a newly discovered “stellar string”, Theia 301, which itself is related to the AB Dor moving group through common membership between their filamentary stars. We conclude in §6 with a brief summary of our findings.

2. THE HD 54236 SYSTEM

HD 54236A is a $V=9.26$ object in the constellation Puppis. It was identified as a member of a common proper motion binary in the first CCDM catalog (Soderblom et al. 1993). It is also listed as a visual binary in the Washington Visual Double Stars catalog (Mason et al. 2001). It was identified as a possible pre-main sequence (PMS) object from the SACY survey (Torres et al. 2006): first through its detection as a strong X-ray source, and then through Li observed in its spectrum. Torres et al. (2006) classified HD 54236A as spectral type G0V, and HD 54236B as spectral type K7V.

The total proper motion is 17.25 ± 0.22 mas yr⁻¹ for both HD 54236 A and B (values from the Gaia archive Gaia Collaboration et al. 2018), and the equivalent width (EW) of the Li line is given in the SACY catalog as 120 mÅ for A and 40 mÅ for B. No uncertainties are provided in the SACY catalog for the Li EW values. Below we report updated precise measurements of the Li EW and abundances for the stars.

HD 54236A is in a fairly crowded part of the sky, and thus all our photometry to date is blended with nearby stars at some level. We will pay special attention in § 3.1 to describing the degree of blending in each set of observations. To clarify the environment, Figure 1 displays a DSS image of the HD 54236 system, the eclipsing binary HD 54236A and its common proper motion (CPM) companion, HD 54236B at a distance of ~ 21 AU. Surrounding, unrelated field stars are also identified. This observational ecosystem includes:

- HD 54236A ($V=9.26$), spectral type $\sim G0$, which is the principal object of study in this paper and which we identify as an eclipsing binary.
- HD 54236B, which is 6.5 arcseconds south of HD 54236A and is $V=13.2$, spectral type $\sim K7$. It is a common proper-motion companion of HD 54236A, and we confirm below that it shares the systemic radial velocity of HD 54236A also.
- The bright star HD 54262, which is 54 arcseconds east of HD 54236A and is $V=9.31$. Based on its reported proper motion of $\mu_\alpha = -55.06 \pm 0.06$ mas yr⁻¹ and $\mu_\delta = -1.36 \pm 0.06$ mas yr⁻¹, compared to the proper motion of the HD 54236 system of $\mu_\alpha = -8.01 \pm 0.06$ mas yr⁻¹ and $\mu_\delta = -15.28 \pm 0.05$ mas yr⁻¹ (*Gaia*), it appears certain that HD 54262 is not associated with the HD 54236 system.
- A very distant (~ 3529 pc; Gaia Collaboration et al. 2018) and faint star ($V = 14.6$) that is 7.4 arcseconds to the north of HD 54236A (TIC 767642478) is not physically associated with the HD 54236 system.

Thus, to our knowledge, the HD 54236 system physically comprises three stars: HD 54236A which we identify below as an eclipsing binary (two stars, unresolved) and HD 54236B as a wide CPM tertiary companion that is visually resolved with a separation from HD 54236A of 6.5 arcseconds.

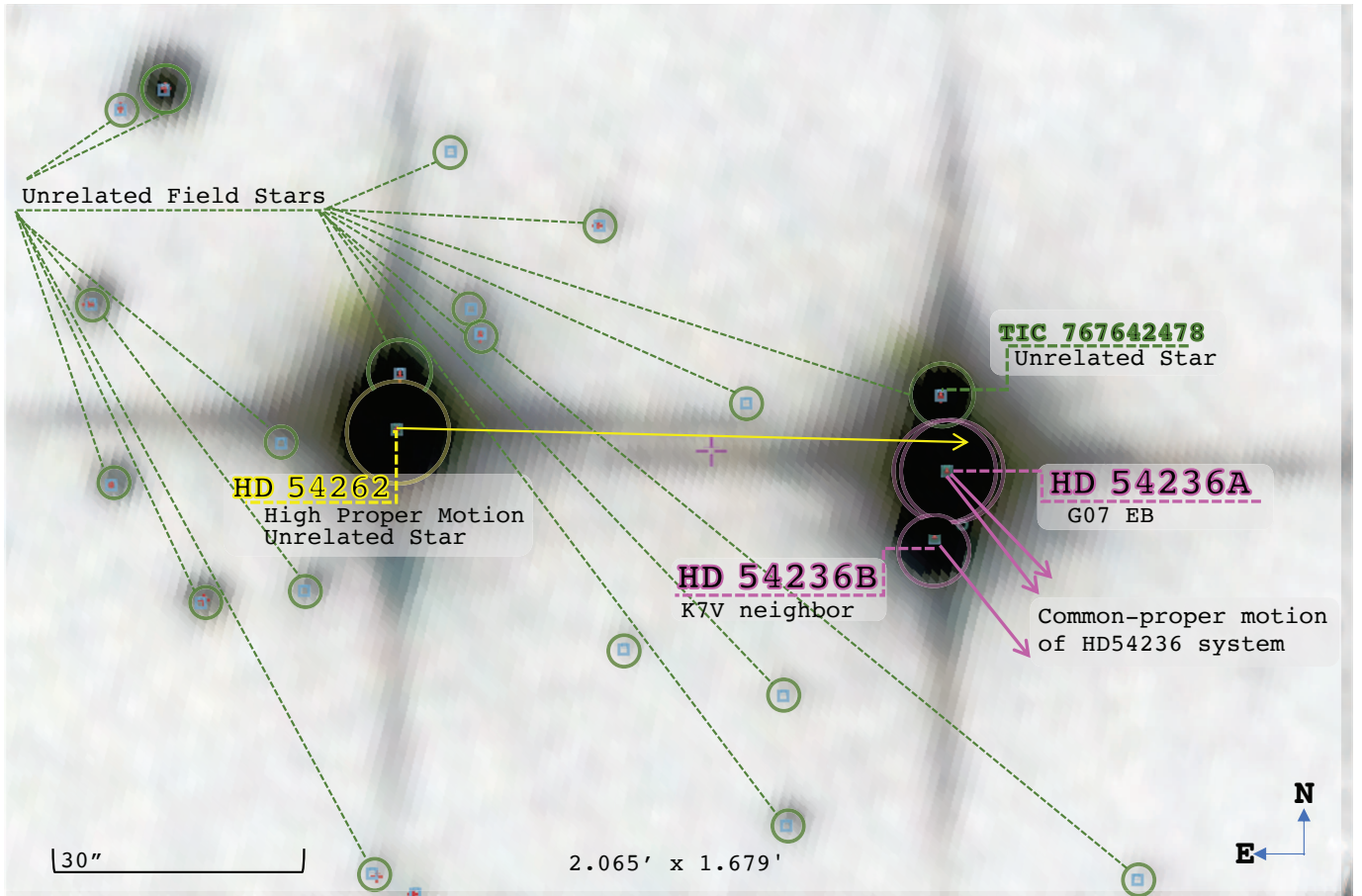


Figure 1. DSS image of the HD 54236 tertiary system and its common-proper-motion is highlighted in fuchsia. The tertiary system includes HD 54236A (the eclipsing binary), and HD 54236B, the CPM tertiary member ~ 6.5 arcseconds south of HD 54236A. Surrounding, unrelated stars (like TIC 767642478, the distant faint star to the north) are shown in green. HD 54262, an unrelated high proper motion star to the east is highlighted in yellow.

3. DATA

3.1. Photometric Observations

3.1.1. KELT-South Photometry

The Kilodegree Extremely Little Telescope-South (KELT-South) is a dedicated exoplanet transit telescope located at the Sutherland observing station of the South African Astronomical Observatory (SAAO). The telescope, hardware, and the primary exoplanet survey is described in Pepper et al. (2012). The KELT observations are taken with a Kodak Wratten #8 red-pass filter, resembling a widened Johnson-Cousins R -band.

KELT-South conducted a commissioning run from Jan 4, 2010, to Feb 19 2010. During that run, KELT-South continuously observed a field centered at $\alpha = 08:16:00$, $\delta = -54:00:00$, with repeated 30 s exposures. After removal of poor-quality images, we have a total of 3,041 images across 29 individual nights. We generated relative photometry from flat-fielded images using a modified version of the ISIS image subtraction package (see also Alard & Lupton 1998; Alard 2000; Hartman et al. 2011), in combination with point-spread function fitting using the stand-alone DAOPHOT II (Stetson 1987, 1990) package, and the SExtractor program (Bertin & Arnouts 1996). A more complete explanation of our pipeline procedures, and the algorithms, are provided in Siverd et al. (2012).

One of the transit candidates was HD 54236A. Although the depth and out-of-eclipse variation of the lightcurve indicated that the target was unlikely to be a transiting planet, the prospect that it represented a bright PMS eclipsing binary prompted us to gather additional data of this target. The KELT light curve of HD 54236A is shown in Fig. 2.

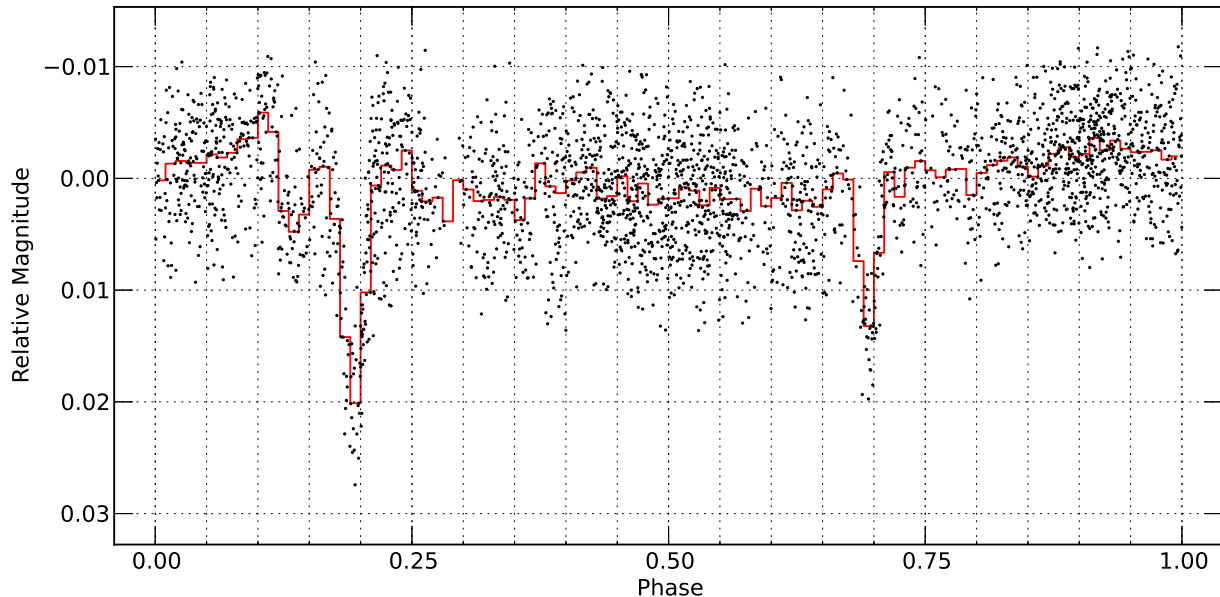


Figure 2. Phase-folded lightcurve of HD 54236A from KELT. Small symbols represent individual measurements, red lines represent the binned light curve.

Because of the very wide-field nature of the KELT observing setup, with the accompanying large pixel scale (23 arcseconds per pixel), the KELT lightcurve of HD 54236A (Fig. 2) is blended with all of the other stars identified in Figure 1. The largest component of blended flux comes from HD 54262, which is about 0.33 mag fainter than HD 54236A. Therefore, the eclipse depths seen by KELT are at least 40% shallower than the true depths.

An initial periodicity analysis yielded a most likely orbital period of ~ 2.4 d. In addition, there is an out-of-eclipse variation of a nearly sinusoidal morphology in the KELT light curve with a best-fit period of 2.3955 d, i.e., slightly shorter period than the orbital (eclipse) period. A more detailed examination of the out-of-eclipse variations is provided by the *TESS* light curve (see below).

3.1.2. *PEST* Photometry

One of the partners of the KELT-South survey is the Perth Exoplanet Survey Telescope (*PEST*), operated by T.G. Tan. *PEST* consists of a 12" Meade LX200 SCT f/10 telescope, with a focal reducer yielding f/5. The camera is an SBIG ST-8XME, with 1.2 arcsec/pixel.

PEST observed HD 54236A on the night of April 25, 2012, for 119 minutes around the predicted time of primary transit in the Cousins *R*-band, although the ephemeris was poor given the elapsed time between the original observations and the *PEST* observations (over 2 years). The observations caught the last hour of the primary eclipse egress plus an hour after the eclipse. This light curve is more pure than the discovery KELT light curve in that it excludes light contamination from HD 54262. The *PEST* light curve does however still include light contamination from the faint visual companion HD 54236B. The raw photometry of the combined HD 54236A/B system was extracted using the C-Munipack software package¹ (written by David Motl) to perform aperture photometry. Relative photometry was derived using a set of three nearby comparison stars via a custom-written program.

The *PEST* light curve is shown in Figure 3, together with the KELT data scaled by a factor of 3 in flux to account for the additional dilution of the KELT data by the high proper motion bright star HD 54262. The addition of the *PEST* photometry allowed us to refine the orbital period from the KELT data because of the expanded time baseline.

3.1.3. *TESS* Photometry

TESS observed HD 54236 (TIC 238162238) in Sectors 6, 7, and 8 from December 15th, 2018, to February 27th, 2019. The 2-minute cadence light curves were processed using the Lightkurve Python module (Lightkurve Collaboration et al.

¹ <http://c-munipack.sourceforge.net/>

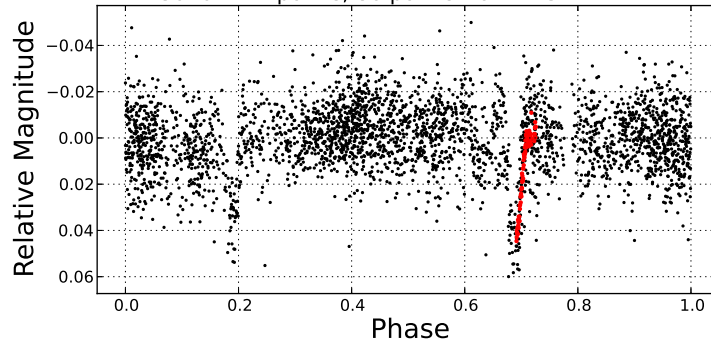


Figure 3. Phase-folded lightcurve of HD 54236A from KELT (*black points*) with the follow-up data from PEST over-plotted (*red points*). Since the KELT data includes the flux from the unrelated high proper motion star HD 54262, the KELT data are multiplied by a factor of 3 to match the egress slope from the PEST data.

2018). We extracted the light curves using the optimized aperture selected by the Science Processing Operations Center (SPOC) pipeline. The mask was chosen to avoid the high proper motion star to the west, HD 54262, from blending the photometry of HD 54236 (see Figure 4). The tertiary star, HD 54236B, remains blended but as it contributes only 2.5% of the flux we do not attempt to correct for it.

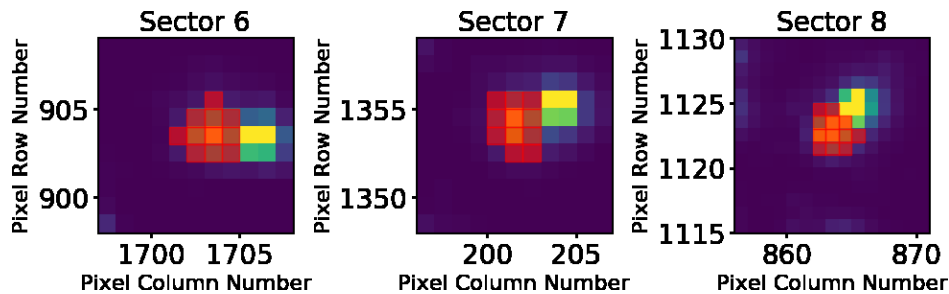


Figure 4. *TESS* Target Pixel File cutouts of HD 54236 for Sectors 6, 7, and 8. The red aperture mask is the optimal aperture from the SPOC pipeline, chosen to avoid the distant faint star to the north, TIC 767642477, from blending the photometry.

To estimate the background, we required a brightness threshold such that the pixels in the Target Pixel File that are 0.1% times the standard deviation below the overall median flux of pixels in the selected aperture. We then subtracted the background from our source signal and normalized by the median flux.

To remove long-term trends and to assist with normalization of the flux baselines between sectors and satellite downlink times, we utilized a Biweighted Midcorrelation filter (via the *Wotan* package; M. et al. 2019). We chose a window size of 3 times the ~ 2.4 d period to ensure at least 3 transits are included in each window and will not be overfitted by the smoothing function. The long-term detrended light curve is shown in Figure 5.

We then utilized the *Astropy* implementation of the Box-fitting Least Squares (BLS) algorithm to estimate the period of the evident out-of-transit variations. We used a period range from 1.5 to 11 d with 10000 steps in frequency and a transit duration range of 1 to 24 hr. In Figure 6, we focused on a region of the BLS periodogram centered on 2.43 d and are able to identify the orbital period of 2.4377 d along with another prominent periodic feature corresponding to a period of 2.3782 d, which we attribute to the rotational period of one or both of the stars in the EB.

To remove this out-of-eclipse variation, we then used a 24-hr window for our smoothing function. In Figure 7, we show the first 10 days of our *TESS* light curve with the trend line that is fit to the flux baseline in red. Since the Biweighted Midcorrelation filter is median-based, it is less sensitive to outliers and ignores the transit events. In Figure 8, we show the final phase-folded *TESS* light curve on the orbital period estimated above from the *TESS* light curve. We report a final system ephemeris combining all of the available light curve data in Section 4.1.

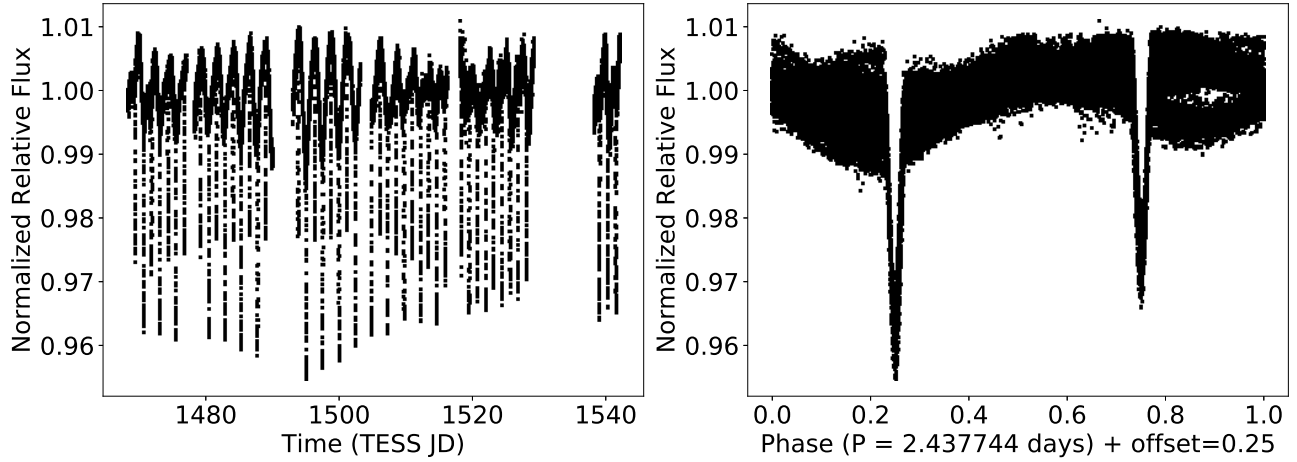


Figure 5. *Left:* TESS light curve of HD 54236 in Sectors 6, 7, and 8. *Right:* Phase-folded TESS light curve.

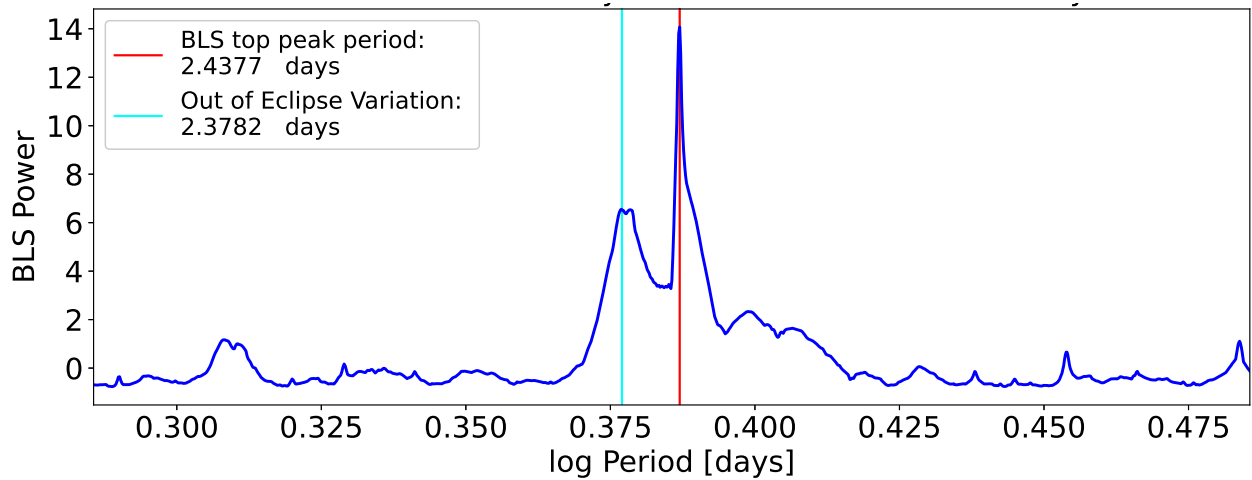


Figure 6. BLS periodogram, showing the most prominent periodic features, corresponding to the eclipse period but also showing a similar but different period of 2.3782 d which we attribute to the stellar rotation period (see the text).

3.2. Spectroscopic Observations

Spectroscopic Observations of the HD 54236 were acquired from the Wide Field Spectrograph (WiFeS) and echelle spectrograph on the ANU 2.3 m telescope from the Australian National University², and, the Goodman High Throughput Spectrograph (Clemens et al. 2004), installed on the f/16.6 Nasmyth platform of the 4.1 m SOUTHERN Astrophysical Research (SOAR) telescope. In what follows, each instrument and the analysis of its spectroscopic observations are described.

3.2.1. ANU 2.3m Spectroscopy

We obtained a single 100-sec exposure of HD 54236A using WiFeS (Dopita et al. 2007) on the ANU 2.3 m telescope at Siding Spring Observatory, Australia. WiFeS is an image slicer integral field spectrograph, where the B3000 grating and the RT560 dichroic were selected for our observations, giving the spectral coverage of 3500–6000Å at a resolution of $\lambda/\Delta\lambda = 3000$. The object spectrum was extracted and reduced with the IRAF³ packages CCDPROC and KPNOSLIT, with the wavelength solution provided by a Ne-Ar arc lamp exposure taken on the same night. The spectrum is flux

² <http://rsaa.anu.edu.au/observatories/siding-spring-observatory>

³ IRAF is distributed by the National Optical Astronomy Observatory, which is operated by the Association of Universities for Research in Astronomy (AURA) under cooperative agreement with the National Science Foundation.

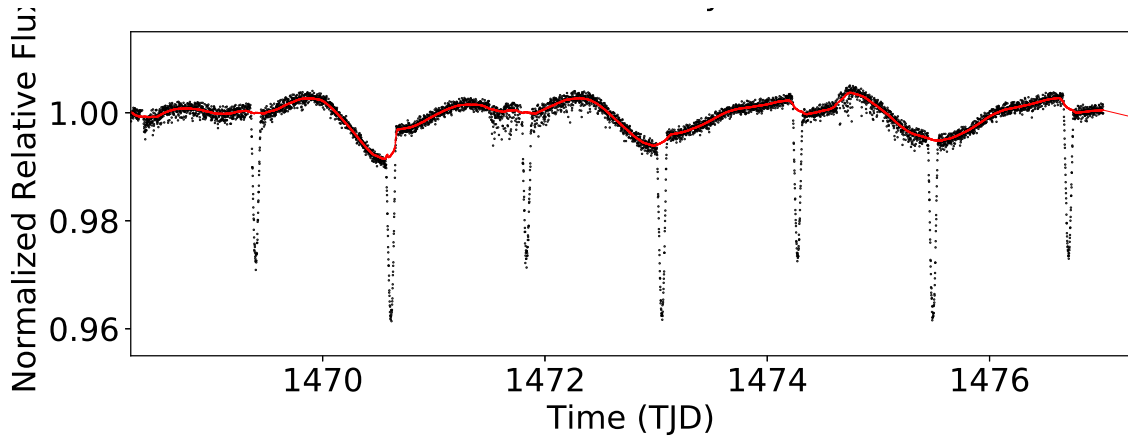


Figure 7. The first 10 days of the *TESS* light curve spanning Sectors 6 to 8, shown in *TESS* Julian Days (TJD). The black points are the *TESS* data and the red line is the Biweighted Midcorrelation filter applied to the flux baseline. We used a window size of 6 hours which equals to 3 times the transit duration reported by BLS.

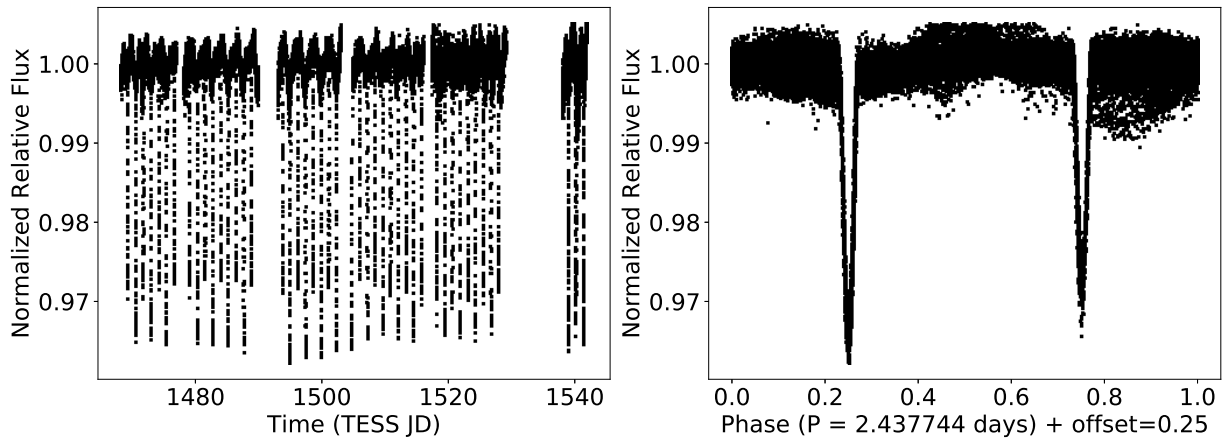


Figure 8. The phase folded *TESS* light curve that was smoothed using a Biweighted Midcorrelation filter as described in §3.1.3. The out-of-transit variations seen in Figure 5 are removed in these data.

calibrated against exposures of spectrophotometric standard stars from Hamuy et al. (1994), employing techniques described in Bessell (1999). The resulting flux-calibrated spectrum had signal-to-noise of $S/N = 300$ per resolution element.

The reduced object spectrum was fitted to a grid of synthetic spectra from Munari et al. (2005), spaced at intervals of 100 K in T_{eff} , 0.5 dex in $\log g$, 0.5 dex in $[\text{Fe}/\text{H}]$, and 0.02 magnitudes in $E(B - V)$. Discrepancies between the object spectrum and the synthetic template are largely due to differences in the flux calibration between them but prevent no analytical obstacle as spectral matching is done based on spectral features, rather than its overall shape. We weighted regions sensitive to $\log g$ variations preferentially, including the Balmer jump, the MgH feature at 4800\AA , and the Mg b triplet at 5170\AA . Details of the data reduction and spectral fitting process can be found in § 3.2.1 of Penev et al. (2013). The resulting derived atmospheric parameters for HD-54236A are $T_{\text{eff}} = 6350 \pm 100$ K, $\log g = 5.0 \pm 0.3$, and $[\text{Fe}/\text{H}] = -0.5 \pm 0.5$ (see Figure 9, top panel). Note that this analysis assumes that HD 54236A is a single star, when in fact it is a binary. We return to a discussion of this in § 4.5.

We also observed the fainter CPM tertiary companion star HD 54236B. The analysis is displayed, as for HD 54236A, in Figure 9 bottom panel, and yields the following stellar parameters: $T_{\text{eff}} = 4400 \pm 200$ K, $\log g = 4.8 \pm 0.35$, $[\text{Fe}/\text{H}] = -0.5 \pm 0.44$ (Bayliss et al. 2013). In addition, from this spectrum we have verified the Li EW of HD 54236A reported by SACY (120 m\AA). We obtain an EW of $140 \pm 20 \text{ m\AA}$ for the Li line at 6708 \AA , representing the blended EW of both stars in the HD 54236 EB.

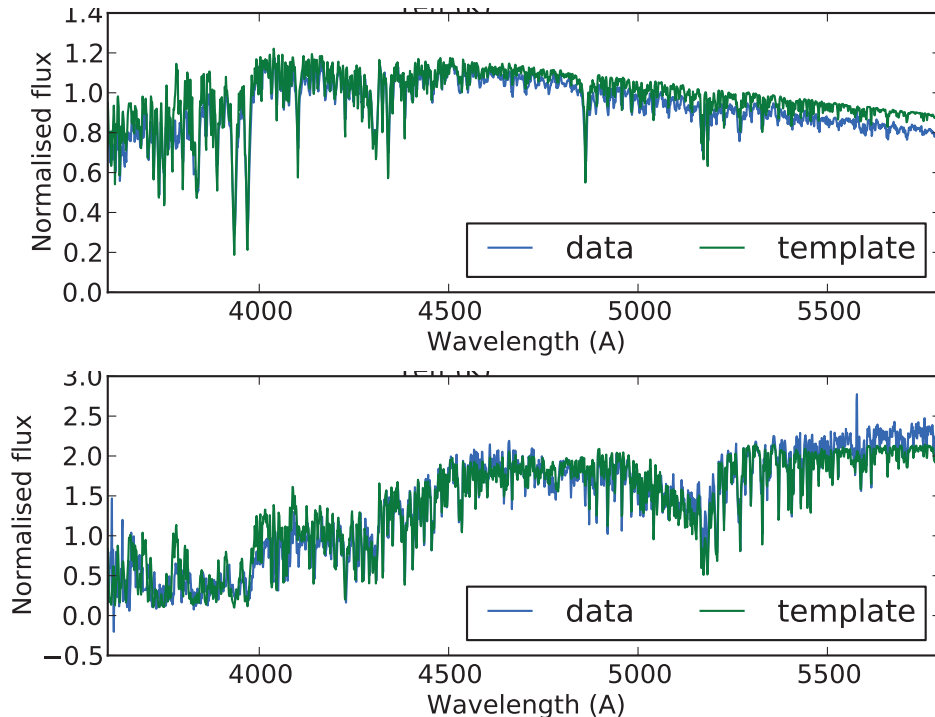


Figure 9. *Top:* Spectral analysis of the stellar parameters of HD 54236A, the eclipsing binary. *Bottom:* Spectral analysis of the stellar parameters of the tertiary member, HD 54236B. The observed spectra for both HD 54236A and HD 54236B are shown in blue, while their respective templates modeled in green. Discrepancies between the target spectra and its template are largely due to differences in flux calibration, however, spectral matching is done based on spectral features rather than overall shape.

The WiFeS spectrograph was also used to measure the radial velocities of the eclipsing stars. One spectrum was obtained on HJD 2456104.838 using WiFeS at medium resolution ($\lambda/\Delta\lambda = 7000$), where both components of the spectroscopic binary were resolved. The observation and data analysis process follows Penev et al. (2013). The velocities were measured via cross correlation as described in the next section, and are reported along with the full set of velocities described below in Table 1.

3.2.2. High-resolution Spectroscopy: Radial velocities

Nine high-resolution observations of HD 54236A were obtained using the ANU 2.3 m echelle spectrograph, at a resolution of $\lambda/\Delta\lambda \approx 23000$, velocity dispersion of $4.0 \text{ km s}^{-1} \text{ pixel}^{-1}$, in the spectral range 4200–6700Å, over 20 echelle orders. The data was reduced with the IRAF package CCDPROC, extracted and normalized using ONEDSPEC. The wavelength solution was provided by Th-Ar arc lamp exposures that bracketed each science exposure. A standard 950 sec exposure of the target yields a signal-to-noise of $S/N = 40$ per resolution element. The instrument setup, observations, and data reduction process are detailed in Zhou et al. (2014).

We cross-correlated the object spectra against a series of radial velocity standard star spectra taken during twilight each night. The cross-correlation peaks for the two spectroscopic components of the object were resolved in the observations, we were therefore able to extract radial velocities for both components in each observation by fitting Gaussians to the two cross-correlation peaks. We take the stronger peak to represent the (more massive) primary component. An example cross-correlation function (CCF) for the observation on HJD 2456057.93945 is shown in Figure 10.

The radial velocity is calculated as the mean over all orders not affected by telluric contamination, weighted by their respective signal-to-noise ratio; the scatter in the measurements over the orders gives the error in the radial velocity measurement for that epoch. The complete set of primary and secondary radial velocities determined from these observations and are summarized in Table 1.

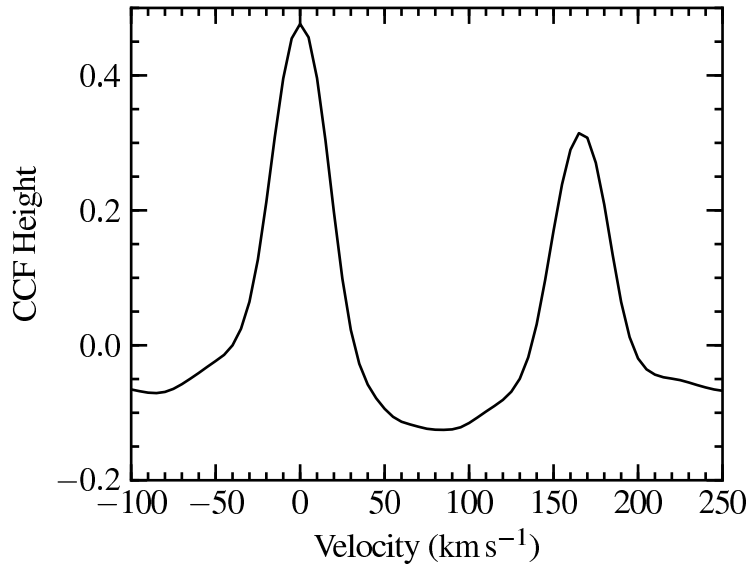


Figure 10. Cross-correlation function for the spectrum taken on HJD 2456057.93945226, with the ANU 2.3 m echelle at $R = 23000$. The CCF shown is the average CCF of the cross correlations from all echelle orders, excluding those with very low cross-correlation heights. The cross-correlations are performed against RV standard star exposures taken on the same night. For clarity, the highest peak (presumed to correspond to higher mass, primary component in the eclipsing binary, has been shifted in this figure to be at 0 km s^{-1} .

Table 1. RV Observations of HD 54236 A

HJD (UTC)	Primary RV (km s^{-1})	Secondary RV (km s^{-1})	Source
2456057.93945	-88.7 ± 1.3	76.9 ± 0.9	ANU 2.3m
2456057.95085	-90.6 ± 1.4	78.9 ± 1.1	ANU 2.3m
2456058.92243	21.7 ± 1.2	-46.3 ± 1.1	ANU 2.3m
2456059.92704	6.6 ± 1.5	-35.2 ± 0.8	ANU 2.3m
2456061.96015	84.9 ± 1.4	-109.1 ± 1.1	ANU 2.3m
2456086.48771	63.4 ± 1.0	-90.4 ± 1.0	SOAR 4.1m
2456087.85052	-55.9 ± 2.0	36.9 ± 1.9	ANU 2.3m
2456087.86683	-54.3 ± 1.6	30.1 ± 2.7	ANU 2.3m
2456088.84221	75.9 ± 1.2	-102.7 ± 1.0	ANU 2.3m
2456088.85501	73.4 ± 1.2	-101.7 ± 1.1	ANU 2.3m
2456104.83853	-68.8 ± 1.1	61.3 ± 1.6	ANU 2.3m

3.2.3. SOAR Spectroscopy

HD 54236 A & B were observed on UT 20120605 and UT 20120607 using the Goodman High Throughput Spectrograph (Clemens et al. 2004), installed on the f/16.6 Nasmyth platform of the 4.1m SOuthern Astrophysical Research (SOAR) telescope. The spectrograph used the 1200 l/mm grating in M5 mode, a 0.46-arcsecond wide slit, a GG-495 blue-blocking filter, imaged onto a 4096×4096 Fairchild CCD detector, having square $15 \mu\text{m}$ pixels ($0.15 \text{ arcsecs/pixel}$). This setup yields a central wavelength of $\simeq 6890 \text{ \AA}$, a wavelength range of $\simeq 6275\text{--}7495 \text{ \AA}$, a spectral dispersion of 0.304 \AA per pixel and a three-pixel resolving power of $R \simeq 7000$ at 6400 \AA . The FWHM of cross-correlated CuHeAr arc lines is 4.7279 pixels or 62.58 km s^{-1} . Using this setup, HD 54236 A and B were separately observed for exposure times of 300- and 900-seconds, respectively, on UT 20120605, and 300- and 600-seconds, respectively, on UT 20120607, resulting in spectra having maximum S/N near to $\text{H}\alpha$ of $\simeq 350$ for HD 54236A and 100 for HD 54236B.

For each target, we measured heliocentric radial velocities and Li I 6708 \AA equivalent widths. CCD instrumental effect removal (such as de-biasing and flat-fielding), as well as the extraction of wavelength calibrated spectra, was

performed using standard IRAF procedures. Heliocentric radial velocities were determined relative to the International Astronomical Union standard stars HR 6468, HR 6859, HD 120223 and HD 126053. Cross-correlation of the velocity standards against one other shows that the zero-point relative to the standard system is accurate to $\sim 0.2 \text{ km s}^{-1}$. The CCF is the average from all echelle orders, excluding those with very low cross-correlation heights and are performed against RV standard star exposures taken on the same night. The radial velocity standard stars on these nights shows that the system is stable to $\simeq 0.5 \text{ km s}^{-1}$ over the course of the night.

The radial velocities for the eclipsing components of HD 54236A are reported with the other radial velocity measurements in Table 1. For the single star HD 54236B, we obtain a systemic velocity of $-12.0 \pm 0.3 \text{ km s}^{-1}$. As shown below, this velocity is consistent with the systemic velocity of the HD 54236A eclipsing binary system.

In order to measure the EW of the Li I 6708 Å resonance lines, the Goodman spectra were first trimmed to 6620–6750 Å and normalized using a 7th-order spline function fit to the continuum. Equivalent widths were measured using both Gaussian fits and direct integration to check for consistency. The region of the spectrum around the Li line is shown in Figure 11. The measured Li EWs for the eclipsing stars in HD 54236A are $66 \pm 6 \text{ mÅ}$ for the primary star and $47 \pm 5 \text{ mÅ}$ for the secondary star. Note that these are the directly observed EWs; below we correct these EWs for the mutual dilution of the two stars’ spectra when we transform these EWs into Li abundances.

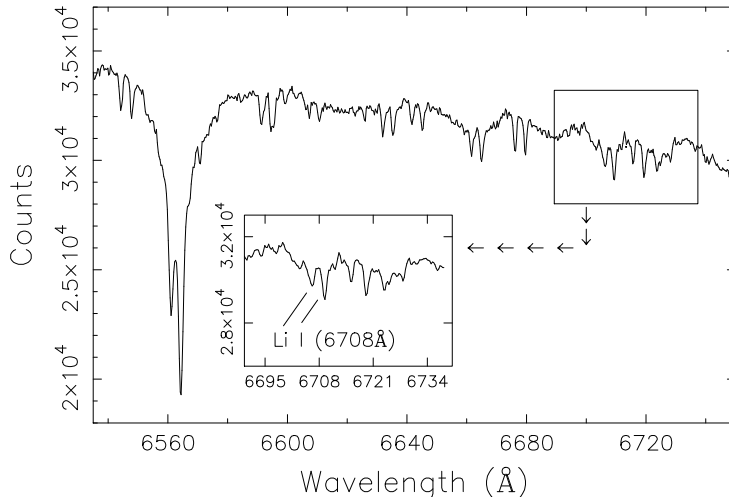


Figure 11. Region of the Li line from the SOAR spectrum.

4. RESULTS

With the above data in hand for the HD 54236 system, including photometric light curves and spectroscopic measurements of the component radial velocities and individual stellar spectra, in this section we determine the orbital parameters as well as constraints on the system age from consideration of the Li absorption and Ca HK emission. To remind the reader, the system comprises three stars, two eclipsing components in HD 54236A and a single CPM star in HD 54236B.

4.1. System Ephemeris

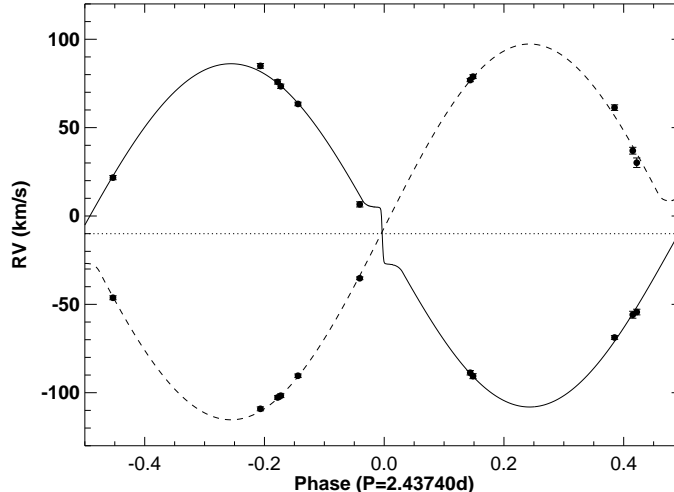
Analysis of all of the available light curve and radial-velocity data together (see §§3.1–3.2), including in particular the KELT, PEST, and the exquisitely precise *TESS* light curves, spanning a total time baseline of more than 10 yr, leads to the final orbital ephemeris determination of $P_{\text{orb}} = 2.43742 \pm 0.00014 \text{ d}$ and $\text{HJD}_0 = 2455199.5980 \pm 0.0021$.

4.2. Orbit Solution

We performed a simultaneous Keplerian orbit fit to the radial velocity measurements of the two eclipsing components of HD 54236A. We fit the ANU and SOAR radial velocities simultaneously, without attempting to introduce any possible systematic offset between the two. Thus, in total we fit 11 primary radial velocities and 11 secondary radial velocities which are listed in Table 1. The resulting orbit solution is shown in Figure 12 and summarized in Table 2. The orbital eccentricity is consistent with zero, which is not surprising given the very short orbital period, hence for the remainder of our analysis we assume a circular orbit ($e \equiv 0$).

Table 2. Orbital Solution of HD 54236 A

q	e	v_γ	$a \sin i$
0.9132 ± 0.012	0.009 ± 0.008	$-10.0 \pm 0.5 \text{ km s}^{-1}$	$9.810 \pm 0.080 R_\odot$


Figure 12. RV solution for HD 54236A: The primary is modeled with the solid line, and the secondary with the dashed line.

4.3. PHOEBE Light Curve Model

The PHysics of Eclipsing BinariEs, (Prsa et al. 2011; Prša et al. 2016) commonly referred to as PHOEBE is an EB modeling code which enhances upon the Wilson-Devinney (Wilson & Devinney 1971) method with improved model fidelity. Functions are available through PHOEBE that provide generation of highly characterized synthetic light curves given orbital and stellar parameters. We invoke PHOEBE to produce synthetic light curves for model fitting to our detrended TESS light curve, adopting the orbital parameters determined from the orbit solution (Section 4.2), such that the principal fitting parameters are the ratio of effective temperatures (T_{ratio}), the sum of the stellar radii (R_{sum}), and the orbital inclination (i). This is appropriate given the circular orbit, where to first order T_{ratio} is set by the relative eclipse depths and R_{sum} is set by the eclipse durations, moderated by i .

We use a Genetic Algorithm (GA) to converge to a model light curve solution. Previous work (see, e.g., Metcalfe 1999) has shown GA techniques to be robust for model fitting eclipsing binary light curves and thus inspired a modified version we utilize here. For computational efficiency we downsample the TESS 2-min cadence light curve by a factor of 15 and run PHOEBE using the Legacy backend, which is markedly faster. The fitting algorithm starts with the generation of an initial random population of 500 model parameter sets [T_{ratio} , R_{sum} , i] in our parameter space, each of which is encoded as a single object representation referred to as a gene. For each model we set the effective temperatures by apportioning the spectroscopically determined average (6350K) according to the flux-weighted sum of the two stars and the current iteration of T_{ratio} . For each gene a corresponding model light curve is computed in PHOEBE, and the χ^2 between the observed and model fluxes is calculated.

To thoroughly explore our parameter space we propagate this population over the course of 20 generations resulting in a total sample of 10,000 models. Iteration of genes from one generation (parent) to the next (child) is done using single point crossover. The members of each parent generation used in the crossover are chosen via roulette wheel until re-population is achieved. The probability of each selection is weighted by the reciprocal of the χ^2 goodness-of-fit metric. To help maintain diversity between generations (i.e., to avoid local minima) we introduce a 10% chance for random mutation within the constraints for the parameters at inception.

After sampling is complete we discard the first 15 generations in order to prevent the lack of convergence in previous generations from contaminating our result. The fitted parameter distributions of the cleaned sample of 2500 models is illustrated in the corner plot (Fig. 13). The distributions are gaussian-like in shape with well determined modal values. Thus, we determined the converged solutions as the mean values of these distributions and the uncertainties

as the standard deviations. The final converged model is shown over our TESS light curve in Figure 14 as well as the residuals between the two. There is evidence of some minor systematics in the residuals of the primary eclipse with an amplitude of ~ 0.003 relative flux units, however this is only $\lesssim 1\%$ of the eclipse depth of ~ 0.035 relative flux units, which we deem acceptable.

We use the fitted T_{ratio} together with the spectroscopically determined flux ratio of 3.0/4.5, and solve Stefan-Boltzmann's Law to obtain R_{ratio} , which with the fitted R_{sum} yields the final individual radii. Similarly, the fitted T_{ratio} together with the final R_{ratio} and the flux ratio yields the final individual temperatures. Finally, using the final i we obtain the stellar masses via the orbit-solution determined $a \sin i$ and q . The final stellar parameters are reported in Table 3.

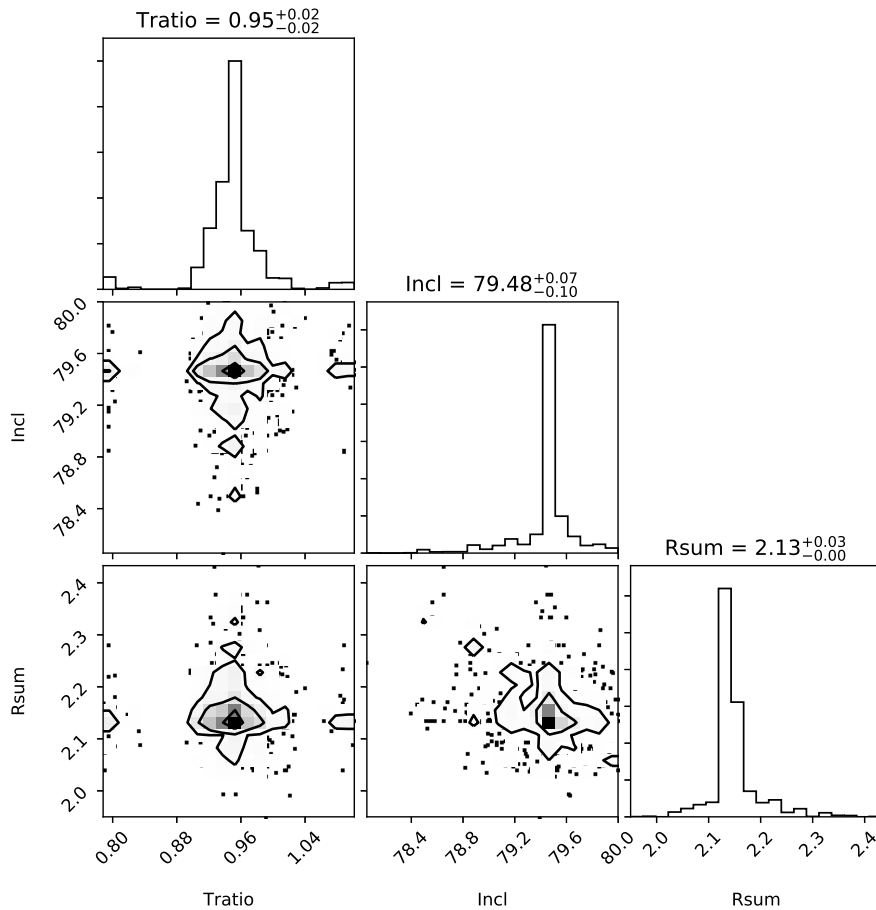


Figure 13. Corner plot of fitted parameters for cleaned sample of 2500 model light curves. Values atop distribution are the median values and the 0.16 & 0.84 quantiles.

Table 3. PHOEBE Fit Parameters and Solutions of HD 54236A

$T_{\text{eff},1}$	$6480 \pm 103 \text{ K}$
$T_{\text{eff},2}$	$6155 \pm 155 \text{ K}$
R_1	$1.128 \pm 0.044 R_{\odot}$
R_2	$1.021 \pm 0.044 R_{\odot}$
i	$79.4 \pm 0.2^{\circ}$
M_1	$1.179 \pm 0.029 M_{\odot}$
M_2	$1.074 \pm 0.027 M_{\odot}$

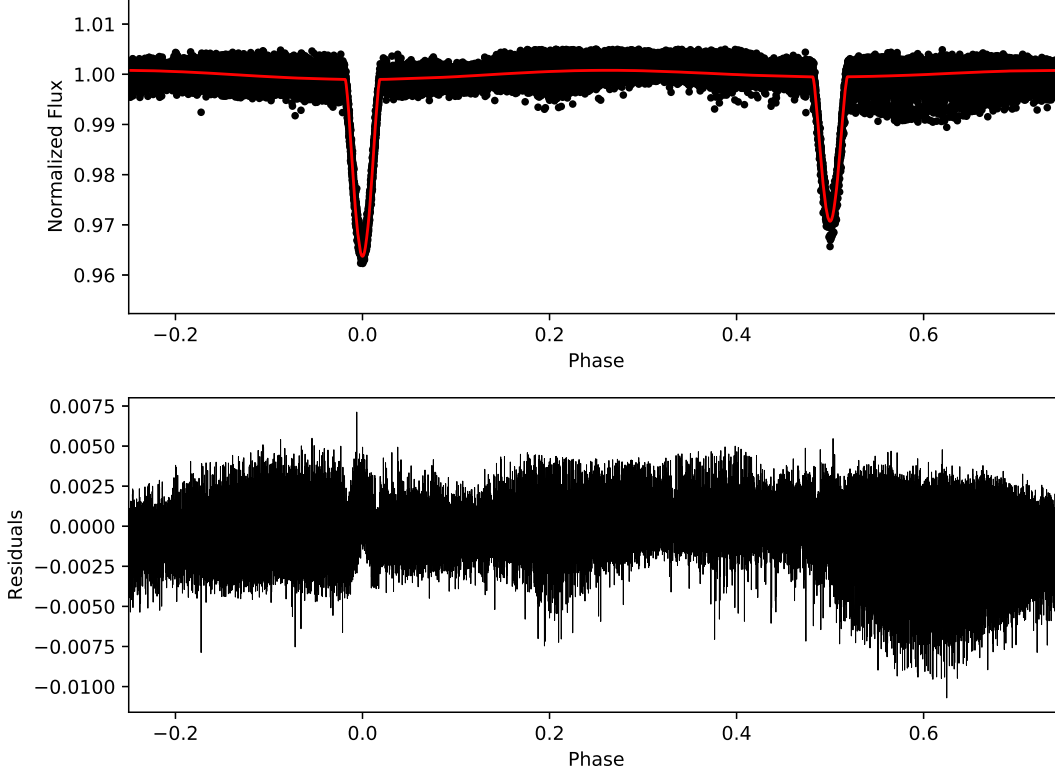


Figure 14. Light curve fitting for HD 54236A using GA converged model solution. There remain some small systematics in the residuals in eclipse, the amplitude of which are of order 1% of the eclipse depths. The final stellar parameters from this solution are listed in Table 3.

4.4. SED Analysis

The radii and effective temperature solutions from the PHOEBE analysis (Table 2) were used in Spectral Energy Distribution (SED) modeling, fitting only for extinction and distance. This is done to ensure that our T_{eff} solutions correctly reproduce the observed shape of the SED, and that the inferred distance from this analysis corresponds to the known *Gaia* distance. From Figure 15 the SED fits for HD 54236A (top) and HD 54236B (bottom) show a very good agreement with our T_{eff} determinations. The *Gaia* distance to HD 54236 is 131.8 ± 0.5 pc, the best-fit distance from the SED analysis is in agreement at 136 ± 6 pc, providing a strong validation of the temperatures and radii that we have determined for both stars in the EB.

For the companion star, HD 54236B, the *Gaia* distance was adopted in fitting the SED to solve for the stellar radius. The stellar radius combined with the $\log g$ yields an estimate for the mass. For the radius we find $0.65 \pm 0.06 R_{\odot}$ and a mass estimate of $0.65 \pm 0.11 M_{\odot}$. These are fully consistent with the empirical relations of Torres et al. (2012) who give a similar but more precise mass estimate of $0.67 \pm 0.04 M_{\odot}$.

4.5. System Age

In order to establish an age estimate for the HD 54236 system, we consider two commonly used stellar chronometers, namely the abundance of Li and the strength of chromospheric activity in the Ca II H&K lines. While the Ca II H&K activity indicator will be enhanced in the eclipsing pair HD 54236A because of their short orbital period and therefore likely enhanced rotation, we utilize the existence of the wide tertiary companion star, HD 54236B, to obtain a clean estimate of the Ca II H&K activity age for the system. This analysis is carried out through the comparison of Ca II H&K spectral features against those of similar effective temperatures from three different open clusters spanning the range of age estimates covered in 4.5.1. Finally, in an attempt to establish association of the system with other nearby stars of similar age, we consider the space motion of the HD 54236 system. For context, in Fig. 16 we show the components of the HD 54236A system in the T_{eff} –Radius plane compared to the Yonsei-Yale stellar evolutionary

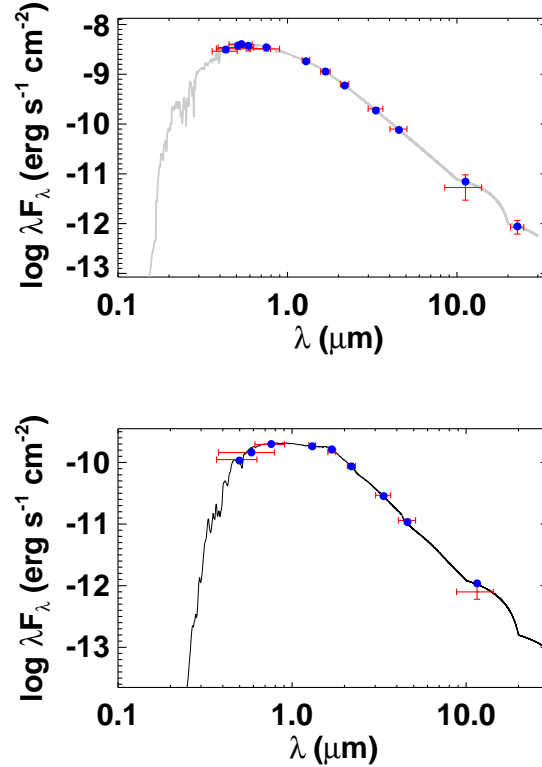


Figure 15. *Top:* SED fit of HD 54236A *Bottom:* HD 54236B SED fit. Red symbols are observed broadband fluxes, curves are the best-fit model atmospheres, and blue symbols are the model fluxes for comparison to the observed fluxes.

tracks (Yi et al. 2001) for the spectroscopically determined $[\text{Fe}/\text{H}]$ of -0.5 . We also represent all three stars—the eclipsing components of HD 54236A and the tertiary HD 54236B—in the H-R diagram plane compared to the PMS evolutionary models of Baraffe et al. (1998). All of which suggest an age near the ZAMS or slightly younger, consistent with the other age diagnostics discussed above.

4.5.1. Lithium

The observed Li EWs for the three stellar components in the HD 54236 system are indicative of a relatively young system age intermediate between the youngest pre-main-sequence clusters and older main sequence clusters. For example, from the analysis of Li EW in young stars of various ages, Aarnio et al. (2008) finds that young stars with K spectral type and ages of ~ 50 Myr have Li EW of 100–200 mÅ, somewhat larger than what we observe in the HD 54236B star (spectral type late K). Therefore it is likely that the HD 54236 system has an age somewhat older than 50 Myr. To determine the Li inferred age of the system more precisely, we analyzed the observed Li EWs for the three stars in HD 54236 in the context of other young clusters.

First, we corrected the observed EWs for the two eclipsing stars to account for the mutual dilution of the two stars’ spectra in our combined light observations. Based on the stars’ final T_{eff} values from our PHOEBE modeling and SED fits, we converted the Li EW into Li abundances, $A(\text{Li})$, using standard curve-of-growth techniques (Soderblom et al. 1993) and applying a NLTE correction (Carlsson & Stein 1994).

The sample from Sestito & Randich (2005) contains 22 clusters spanning a range of ages from ~ 5 -Myr to ~ 6 –8 Myr, for our comparison, we gathered $A(\text{Li})$ for several of these open clusters ranging in age from 35 Myr to 1.2 Gyr and follow the same curve-of-growth and NLTE correction in our abundance calculation method for the HD 54236 system. The stellar censuses for our comparison clusters shown in 17 are as follows, in the young clusters with ages less than ~ 100 Myr: NGC 2547 contains 7 stars, IC 2391 has 6, IC 2602 contains 31 and α Per contains 39 stars. In the ZAMS clusters, with ages ~ 100 Myr are the Pleiades with its seven sisters, Blanco 1 which consists of 17 stars, and M35 with a total of 27. The intermediate comparison clusters have ages of ~ 200 –300 Myr and are represented by NGC 2516,

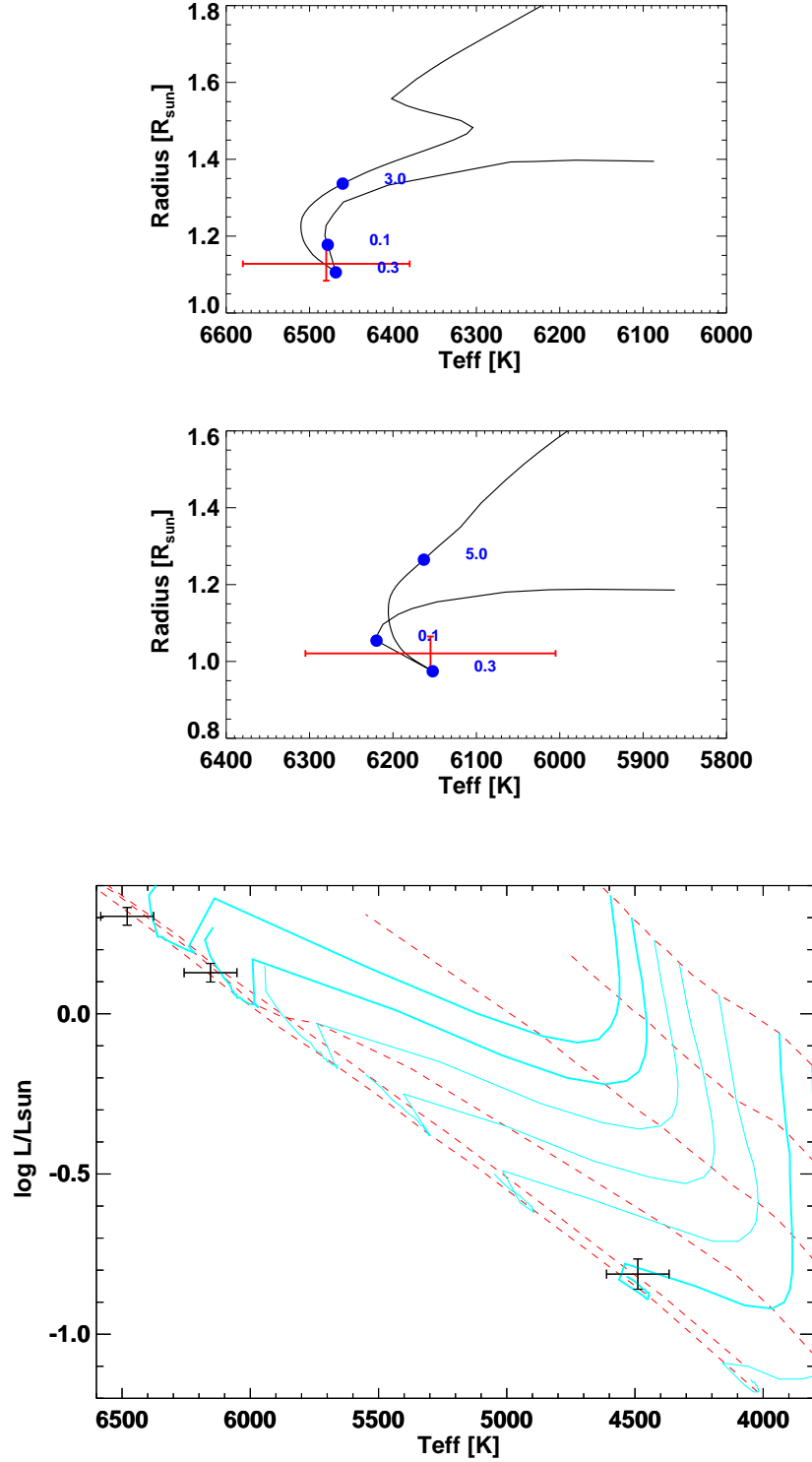


Figure 16. *Top:* T_{eff} -Radius diagram for the primary star of the HD 54236A system. *Middle:* T_{eff} -Radius diagram for the secondary star of the HD 54236A system. Both are in the T_{eff} vs Radius plane and show the Yonsei-Yale stellar evolutionary tracks (Yi et al. 2001), which suggest an age for HD 54236A near the ZAMS (which occurs at an age of 300 Myr in these models) and roughly consistent with an age of 225 ± 50 Myr as determined from other age diagnostics. (*Bottom:*) H-R diagram showing all three components of the HD 54236 system (black symbols) compared to the PMS evolutionary models of Baraffe et al. (1998); shown are isochrones at ages of 1, 3, 10, 30, 100, and 300 Myr (red dashed lines) and tracks for masses of 0.6–1.2 M_{\odot} in increments of 0.1 M_{\odot} (blue curves).

M34 and M7 or NGC 6457 which have 22, 38, and 24 stars respectively. The oldest clusters used for comparison were of ages greater than ~ 400 Myr, these included the UMa Group with 14 stellar members, NGC 6633 with 22 stars, Coma Ber with roughly 40 stars forming its distinctive V shape, Hyades containing 14 stars, and NGC 752, the oldest comparison, having 5 members. The data set used in Sestito & Randich (2005) (and used for comparison in this work) are a collection of independent results from a variety of authors using a degree of models to investigate the evolution of Lithium abundances and their associated timescales.

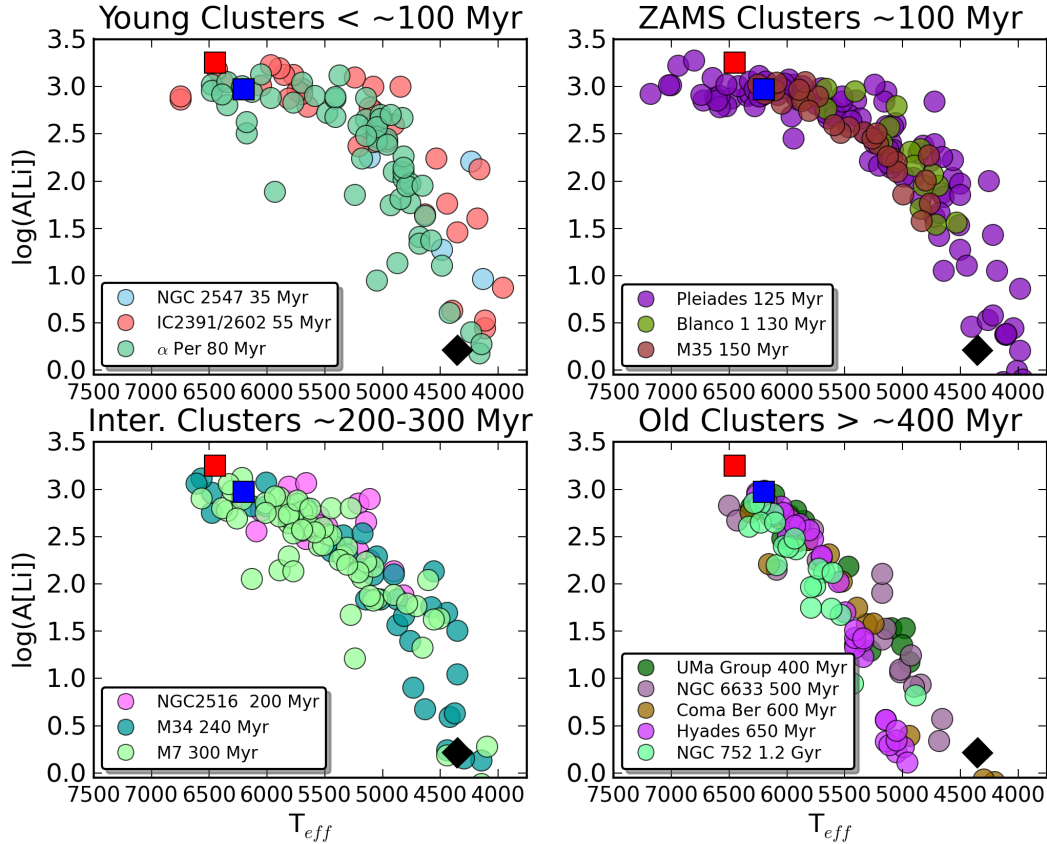


Figure 17. Lithium abundance analysis for a range of ages of clusters: Comparison of EW of lithium abundances from the HD 54236 system to several different clusters ranging in age from 35 Myr to 1.2 Gyr (sample clusters and their parameters are from Sestito & Randich 2005).

From these comparisons we can see that the stellar components in the HD 54236 system (shown with red and blue squares for the primary and secondary stars in the eclipsing binary primary HD 54236A) are indicative of a relatively young age: between PMS clusters and older main sequence clusters.

From visual inspection of Fig. 17, it is clear that the three stars' $A(\text{Li})$ generally follow the trend with T_{eff} observed in young clusters with ages of 100–400 Myr. To constrain the likely age more precisely, we calculated the χ^2 probability of the three stars' $A(\text{Li})$ agreement with each of the comparison clusters shown in the figure. We obtain the following probabilities for the HD 54236 system Li abundances: $P(\text{age} < 100 \text{ Myr}) = 0.03$, $P(\text{age} \sim 100 \text{ Myr}) = 0.09$, $P(\text{age} 200\text{--}300 \text{ Myr}) = 0.40$, $P(\text{age} > 300 \text{ Myr}) < 0.01$. Therefore, statistically the pattern of $A(\text{Li})$ with T_{eff} observed for the three stars in HD 54236 is most consistent with an age of 200–300 Myr. However, a younger age of ~ 100 Myr cannot be entirely ruled out on the basis of the Li abundances alone.

4.5.2. *Ca H & K*

The strength of the emission cores in the H & K lines of Ca II near 3950Å are a commonly used tracer of chromospheric activity and thus, through the empirical rotation-activity relationship of FGK dwarfs, can be used as an age indicator. Given the short orbital period of the eclipsing pair in HD 54236A, it is a good assumption that the two stars have tidally interacted and therefore the stars are likely to have their current rotation governed not by the rotation-activity-age relation, but rather by tidal synchronization with the orbit. Indeed, we observe a roughly sinusoidal variation in the eclipsing system light curve at very nearly the orbital period (see § 3.1), confirming that the stars likely rotate at very nearly the orbital period due to their close separation. Current rotation-activity-age relationships (in this case the age- R'_{HK} relationship) are based on single-star angular momentum evolution, so this rules out using the HD 54236A system to determine the system age using chromospheric activity measures.

Fortunately, the single K-dwarf star in the system (HD 54236B) *can* be used for this purpose. We utilize the high S/N spectrum obtained with the ANU WiFeS spectrograph. Both because our spectrum was not absolutely flux calibrated and because the late spectral type of HD 54236B places it beyond the calibration of existing age-activity relationships (e.g. Wright et al. 2011; Mamajek 2008), we have instead simply compared our observed spectrum with suitable late-type standards from several young clusters.

In Figure 18, we plot the WiFeS spectrum of the Ca II H&K spectral region for HD 54236B against stars with similar effective temperatures ($4200K \leq T_{eff} \leq 4520K$) from three different open clusters spanning the same range of ages found in our analysis of the Li abundances in the previous section 4.5.1.

The open cluster spectra were taken from the Keck HIRES and VLT UVES public archives and convolved down to match the lower resolution of the WiFeS observation. We performed a manual examination of the available spectra to confirm that the open cluster stars plotted are typical in their level of activity for their respective ages.

The agreement of the comparison open cluster spectra to the HD 54236B spectrum outside of the Ca II H&K lines is good evidence that the selected open cluster stars are of appropriately similar spectral type. This is important because the change in level of activity in this age range is a fairly sensitive function of spectral type. For instance, at Pleiades age the Ca II H&K emission cores transition from very strongly present for $T_{eff} \lesssim 4300$ K to modest (at this spectral resolution) for $T_{eff} \gtrsim 4475$ K, a change of only 175 K. Nevertheless, all of the Pleiades show significant Ca II emission (even at the WiFeS resolution) at levels significantly higher than observed in HD 54236B. In contrast, there is also agreement between the observed mild emission in HD 54236B and the M7 comparison star (Bottom panel, 18). Together, these comparisons strongly imply an age for HD 54236B (and therefore of the HD 54236 system) that is older than the Pleiades (~ 130 Myr) and younger than M7 (~ 300 Myr).

4.5.3. Isochrone fitting

Ancillary age estimates for HD 54236 B are fitted using photometry and MIST stellar evolutionary models by MINESweeper (for extensive details on the fitting procedure, including priors used in the inference, see Cargile et al. 2019). Using a Bayesian approach, MINESweeper estimates stellar parameters from MIST stellar evolutionary models (Choi et al. 2016). MINESweeper employs multi-nested ellipsoid sampling (due to its efficiency in sampling multimodal likelihood surfaces like stellar isochrones; Feroz et al. 2019) and utilizes optimized interpolation following Dotter (2016). Fitting *Gaia* DR2, 2MASS, and UNWISE photometry for HD 54236B, MINESweeper and the latest MIST stellar evolutionary models yield an age estimate of 149^{+173}_{-77} Myr for HD54236 B, in agreement with our other age estimators outlined above. Being that HD 54236B is a single star, binarity is not an added complication to fitting and, having lower mass than its EB companion is also less evolved than the HD 54236A EB, therefore, HD 54236B's position on in HR diagram space is more sensitive to the system's age.

4.5.4. Summary of Age Estimates

Our observation of the Ca II H&K emission in the HD 54236B K-dwarf star implies an age for HD 54236B (and therefore of the entire HD 54236 system) that is clearly older than the Pleiades (~ 130 Myr) and clearly younger than M7 (~ 300 Myr). This result is in excellent accord with that inferred from the Li abundances of all three stars in the HD 54236 system, for which we obtained a most likely age of 200–300 Myr. As the Li results more clearly rule out an age as young as 130 Myr and the Ca II H&K results more clearly rule out an age as old as 300 Myr, we adopt a most likely system age of 225 ± 50 Myr on the basis jointly of the Li abundances of all three stars and the Ca II H&K emission of the HD 54236B component. This adopted most likely system age of 225 ± 50 Myr is also in agreement with the latest MIST models projected age estimate of 225 ± 50 Myr.

5. DISCUSSION: MEMBERSHIP, STELLAR STRINGS, AND AB DOR

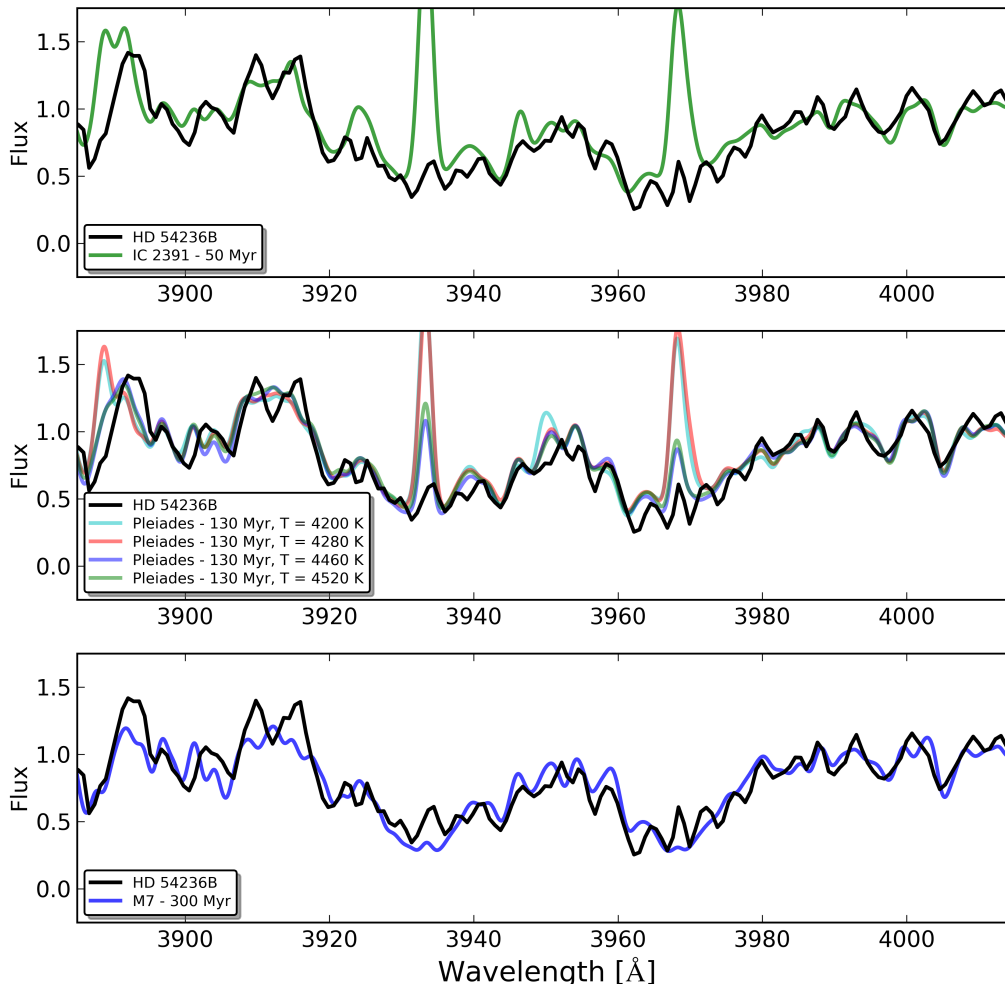


Figure 18. Ca II H&K analysis of the WiFeS spectrum for HD 54236B against stars with similar T_{eff} from three different open clusters spanning the range of ages estimated from the Li abundances in §4.5.1. Against the Ca II H&K analysis for HD 54236B (black line). *Top:* comparison with IC 2391 (age ~ 50 Myr). *Middle:* comparison with Pleiades (age ~ 130 Myr with a range of T_{eff} from 4200 K - 5420 K). *Bottom:* Comparison with M7 (age ~ 300 Myr). The open cluster spectra were taken from Keck HIRES and VLT UVES public archives and convolved to match the resolution of the WiFeS observation of HD 54236B. Taken together, these comparisons strongly imply an age of HD 54236B older than the Pleiades (~ 130 Myr) and clearly younger than M7 (~ 300 Myr).

Gaia DR2 parallax estimates (Bailer-Jones et al. 2018) of HD 54236A puts it at a distance of 133 pc. The galactic space velocity is calculated using the *Gaia* distance, proper motion and radial velocity estimates following Johnson & Soderblom (1987). The *UVW* velocities for the HD 54236 system are calculated using astrolibR Chakraborty & Feigelson (1995) and are listed in Table 4.

Table 4. Galactic Motions of HD 54236A

Parallax	U	V	W
7.56 ± 0.024	$9.07 \pm 0.61 \text{ kms}^{-1}$	$9.54 \pm 0.36 \text{ kms}^{-1}$	$-4.97 \pm 0.23 \text{ CPM kms}^{-1}$

No membership to any population has been established HD 54236 to date. Indeed, the BANYAN Σ Multivariate Bayesian Algorithm (Gagné et al. 2018) reports 0% probability of this source being associated with any of the 27

nearby moving groups that the algorithm considers, based on its *Gaia* DR2 distance and proper motion estimates (Gaia Collaboration et al. 2018; Bailer-Jones et al. 2018).

Nonetheless as the number of known co-moving groups has grown significantly in the recent years, we search for other possible candidate populations from which HD 54236A may have originated. In particular, we perform a cross-match against Kounkel & Covey (2019); Kounkel et al. (2020) catalog, searching for the nearest moving group of which this source may be the most likely member. Examining the sources located closer than $\pi > 6$ mas, with position within 10 degrees, and having proper motions 8 mas yr^{-1} of the source, only one group appears to be close, Theia 301, making it the most likely progenitor.

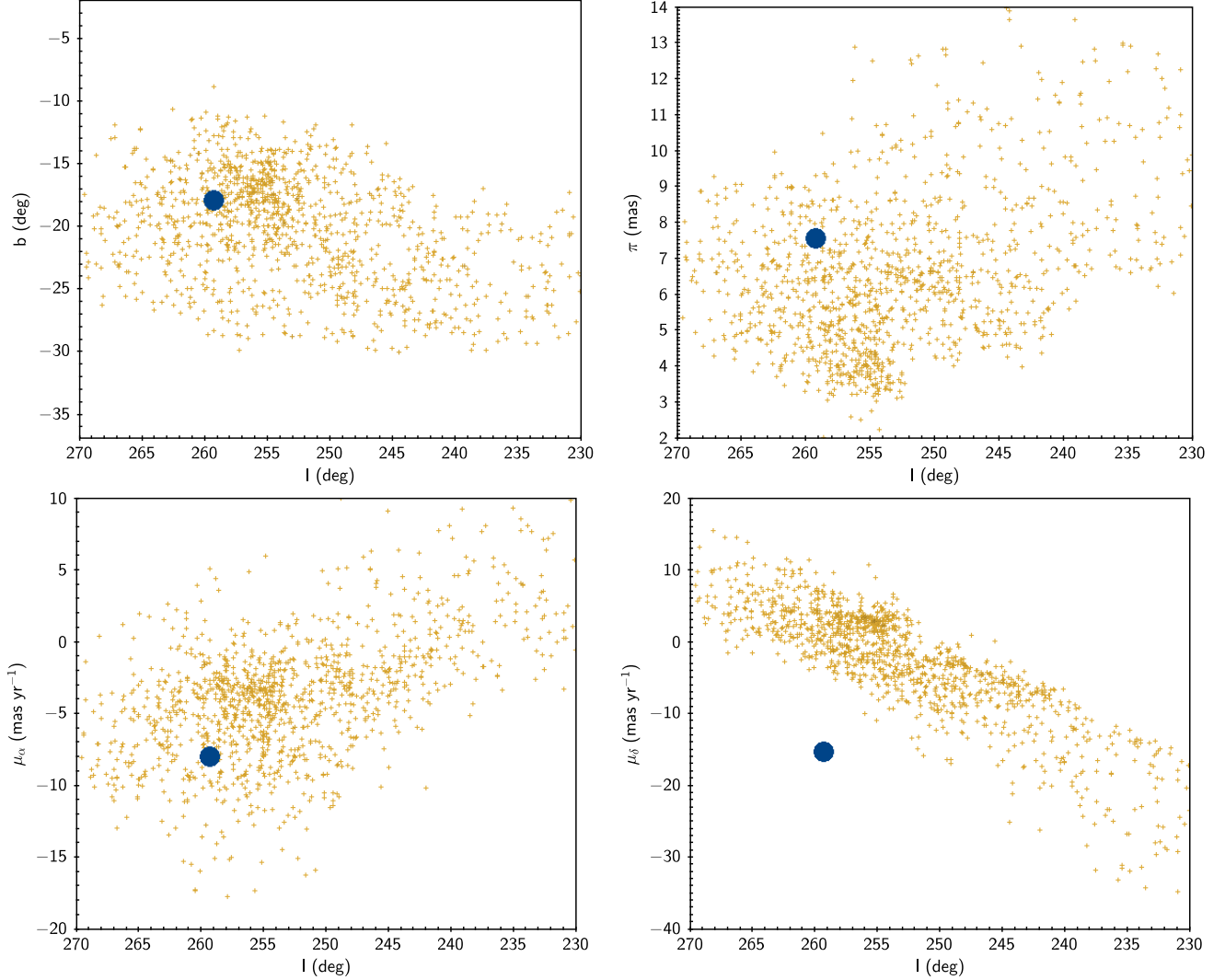


Figure 19. Phase space of HD 54236A relative to the phase space of Theia 301.

Examining the full phase space correlation between the source and the population as a whole, HD 54236A has good agreement with the 3-dimensional spatial distribution of Theia 301, as well as with μ_α (Figure 19). Greater discrepancy is found in μ_δ , where the source is offset by almost $\sim 10 \text{ mas yr}^{-1}$ (6 km s^{-1}). Such an offset could be due to multiplicity of HD 54236A affecting the astrometric solution, or due to a dynamical evolution of the population over time, gaining sufficient speed over the initial conditions to no longer be recoverable in phase-space clustering.

Recent kinematic analyses have led to new associations being made for co-moving groups of Ursa Major (e.g., Gagné et al. 2020) and 32 Ori (e.g., Stauffer et al. 2020). Similarly, we find that a possible ancestral link exists between the AB Dor moving group and Theia 301. Six listed members of the AB Dor association also have membership to Theia 301 (Messina et al. 2010). Connection between the stellar censuses of Theia-301 and AB Dor are tenuous as

so few members of AB Dor are known at distances farther than 80 pc and clustering from Kounkel & Covey (2019) struggles to identify members of moving groups within 100 pc. The observational knowledge gaps in established AB-Dor members beyond 80 pc and clustering within 100 pc converge where we would expect to find shared stellar members between these associations. Even so, there have been 6 stars from Messina et al. (2010) that are listed as members of AB Dor are also members of Theia 301, serving as a bridge between the two populations. The two populations are independently estimated to have roughly the same ages. The age of Theia 301 obtained from the population isochrone fitting is 8.29 ± 0.16 dex, i.e, 134–280 Myr. The age of AB Dor moving group is estimated at 130–200 Myr (Bell et al. 2015). Both are consistent with the age of HD 54236 derived through Li I (§4.5.1) and Ca II (§4.5.2) abundances.

The age of the AB Dor association’s namesake, AB Dor, has been a subject of debate since the findings of Close et al. (2005) estimated the age of the lowest-mass component of the system, AB Dor C, to be only ~ 50 Myr. That same year, Luhman et al. (2005) reported a conservative age range of AB Dor C as 75–150 Myr. When the Close et al. (2005) more youthful age estimate of ~ 50 Myr is used, the luminosity of AB Dor C appears highly discrepant with stellar evolution models predictions. However, when an older age like those suggested by Luhman et al. (2005) and Barenfeld et al. (2013) is used, much of the luminosity discrepancy disappears. Assuming that HD 54236 is indeed a member of Theia 301, and further that Theia 301 is linked to the AB Dor association, our robust age estimates of HD 54236 through lithium abundances (see §4.5.1) and Ca II H&K (§4.5.2) would in turn imply an age for AB Dor that agrees with older age estimates. Our age estimate of ~ 225 Myr being applied to AB Dor C mitigates its luminosity problem.

6. SUMMARY AND CONCLUSIONS

We have shown that HD 54236 is a hierarchical triple system comprising HD 54236A as a previously unknown EB with stellar masses of $1.18 M_{\odot}$ and $1.07 M_{\odot}$, and the late-K type star HD 54236B as a wide CPM tertiary, with estimated mass $0.5\text{--}0.6 M_{\odot}$. We have furthermore shown that the system is young, with a most likely system age of 225 ± 50 Myr from joint consideration of the lithium abundances measured in the three stars and the strength of the Ca II H&K chromospheric activity index. The system age is determined independently from the lithium abundances and Ca II H&K activity to be 225 ± 50 Myr. Using a number of photometric observations for tertiary member HD54236 B, MINESweeper and the latest MIST stellar evolutionary models, yield an age estimate of 149_{-77}^{+173} Myr for HD 54236B providing additional credence to our reported age estimate. At this age, the solar-mass eclipsing component stars (HD 54236A) are very nearly zero-age main sequence stars, and the wide low-mass tertiary companion (HD 54236B) is near the end of its PMS evolution. All solutions from our analysis are collected in 5.

Table 5. HD 54236 System Solutions

$T_{\text{eff},1}$	$6480 \pm 103 K$
$T_{\text{eff},2}$	$6155 \pm 155 K$
R_1	$1.128 \pm 0.044 R_{\odot}$
R_2	$1.021 \pm 0.044 R_{\odot}$
M_1	$1.179 \pm 0.029 M_{\odot}$
M_2	$1.074 \pm 0.027 M_{\odot}$
i	$79.4 \pm 0.2^{\circ}$
q	0.9132 ± 0.012
e	0.009 ± 0.008
v_{γ}	$-10.0 \pm 0.5 \text{ km s}^{-1}$
$a \sin i$	$9.810 \pm 0.080 R_{\odot}$
Parallax	$7.56 \pm 0.024 \text{ mas}$
U	$9.07 \pm 0.61 \text{ km s}^{-1}$
V	$9.07 \pm 0.61 \text{ km s}^{-1}$
W	$-4.97 \pm 0.23 \text{ km s}^{-1}$

The HD 54236 system is also interesting from the standpoint of its dynamics, by virtue of representing a tight EB with orbital period of 2.4 d, with a wide tertiary companion that remains unaffected by the "fountain of youth" which may exist in EBs close enough to enhance their stellar rotation. The wide tertiary companion also represents a statistically

valuable object in stellar multiplicity, and the evolution of three-body tidal effects. For example Tokovinin et al. (2006) finds that, among close binary star systems with orbital periods less than 3 d, the fraction with wide tertiaries is 96%. This promotes three-body dynamics as the primary mechanism for hardening short-period binaries, such as the short period EB HD 54236A and its tertiary member, HD 54236B. Indeed, there may be indications of previous and ongoing dynamics in the HD 54236 system. In particular, our observation of out-of-eclipse variations on a period very similar to but slightly shorter than the EB orbital period indicates that at least one component of the eclipsing binary HD 54236A is not rotationally synchronized with the binary orbit, and therefore should still be experiencing tidal effects. Later observations of the EB HD 54236A would be expected to have an out-of-eclipse variation closer to the period as rotational-orbital synchronization is achieved.

The HD 54236 system previously had no known stellar association to which it might belong. When using the BANYAN Σ Multivariate Bayesian Algorithm (Gagné et al. 2018) with the *Gaia* DR2 distance estimates and proper motion information (Bailer-Jones et al. 2018), HD 54236 was found to have 99% probability of being a field star. That is, every known (as of 2018) stellar association within 150 pc has a nearly 0% probability of having HD 54236A among its members. Additionally, its *Gaia* radial velocity estimates were not similar to radial velocity estimates of the systems considered by BANYAN Σ . However, the Kounkel & Covey (2019); Kounkel et al. (2020) catalog presented newly discovered stellar associations, including “stellar strings”, and found a likely membership to the stellar string Theia 301, which has an estimated kinematic age that is also in very good agreement with our independent age estimate for HD 54236.

Finally, the AB Dor association (and thus AB Dor itself) appears to be linked both kinematically and through a number of shared stellar members to this newly discovered “stellar string” Theia 301. Therefore, the age of ~ 225 Myr that we have found for HD 54236 (and Theia 301) would imply that the AB Dor system also shares this age. Indeed, applying our age estimate to AB Dor itself alleviates reported tension between observation and theory that arises for the luminosity of AB Dor C, when younger age estimates (~ 50 Myr) are used.

Software: C-Munipack (<http://c-munipack.sourceforge.net/>), ISIS image subtraction package (Alard & Lupton 1998; Alard 2000; Hartman et al. 2004), SExtractor (Bertin & Arnouts 1996), DAOPHOT II (Stetson, Davis, & Crabtree 1990), IRAF (Tody 1986, Tody 1993), MINESweeper (Cargyle et al. 2019), MIST (Choi et al. 2019), Lightkurve; s Python package for Kepler and *TESS* data analysis (Lightkurve Collaboration, 2018), astrolibR; used to convert *Gaia* distance, proper motion and radial velocity to galactic coordinates (Chakraborty, Feigelson, & Babu 2014)

ACKNOWLEDGMENTS

We thank the reviewer for a constructive report and helpful feedback. J=MC² would like to thank Erika McIntire, Nicole Megetarian & S. J. Clark for their continued empowerment of a mother in STEM. K.G.S. acknowledges NSF grant AST-1009810. We thank A. Aarnio for independently checking our calculation of the *UVW* space motion of the system. We also gratefully acknowledge Jaci Cloete and Piet Fourie for their technical assistance in the operation of the KELT-South telescope at the South African Astronomical Observatory. This research has made use of the SIMBAD database, operated at CDS, Strasbourg, France.

REFERENCES

- Aarnio, A.-N., Weinberger, A.-J., Stassun, K.-G., Mamajek, E.-E., & James, D.-J. 2008, *AJ*, 136:6, 2483 , doi: 10.1088/0004-6256/136/6/2483
- Alard, C. 2000, *Astronomy and Astrophysics Supplement*, 144, 363 , doi: 10.1051/aas:2000214
- Alard, C., & Lupton, R.-H. 1998, *ApJ*, 503:1, 325 , doi: 10.1086/305984
- Bailer-Jones, C.-A.-L., Rybizki, J., Fouesneau, M., Mantelet, G., & Andrae, R. 2018, *AJ*, 152:58, 11, doi: 10.3847/1538-3881/aacb21
- Baraffe, I., Chabrier, G., Allard, F., & Hauschildt, P. H. 1998, *A&A*, 337, 403. <https://arxiv.org/abs/astro-ph/9805009>
- Barenfeld, S.-A., Bubar, E.-J., Mamajek, E.-E., & Young, P.-A. 2013, *ApJ*, 766:6, 7, doi: 10.1088/0004-637X/766/1/6
- Bayliss, D., Zhou, G., Penev, K., et al. 2013, *AJ*, 146:113, 11, doi: 10.1088/0004-6256/146/5/113
- Beatty, T.-G., Pepper, J., Siverd, R.-J., et al. 2012, *The Astrophysical Journal Letters*, 756:L39, 6, doi: 10.1088/2041-8205/756/2/L39
- Bell, C.-P.-M., Mamajek, E.-E., & Naylor, T. 2015, *MNRAS*, 454, 593 , doi: 10.1093/mnras/stv1981
- Bertin, E., & Arnouts, S. 1996, *Astronomy and Astrophysics Supplemental Series*, 117, 393 , doi: 10.1051/aas:1996164
- Bessell, M.-S. 1999, *Publications of the Astronomical Society of the Pacific*, 111:765, 1426, doi: 10.1086/316454
- Cargile, P. A., Conroy, C., Johnson, B. D., et al. 2019, arXiv e-prints, arXiv:1907.07690. <https://arxiv.org/abs/1907.07690>
- Carlsson, M., & Stein, R.-F. 1994, *ApJ*, 440:L29, 4, doi: 10.1086/187753
- Chakraborty, A., & Feigelson, E.-D. 1995, *Astronomy Users Library: Package astrolibr*
- Choi, J., Dotter, A., Conroy, C., et al. 2016, *ApJ*, 823, 102, doi: 10.3847/0004-637X/823/2/102
- Clemens, C.-J., Crain, A. J., & Anderson, R. 2004, *Ground-based instrumentation for Astronomy, Proceedings*, 5492, doi: 10.1117/12.550069
- Close, L. M., Lenzen, R., Guirado, J. C., et al. 2005, *Nature*, 433, 286, doi: 10.1038/nature03225
- Collins, K. A., Eastman, J. D., Beatty, T. G., et al. 2014, *AJ*, 142:2, 18, doi: 10.1088/0004-6256/147/2/39
- Dopita, M., Hart, J., McGregor, P., et al. 2007, *Ap&SS*, 310, 255, doi: 10.1007/s10509-007-9510-z
- Dotter, A. 2016, *ApJS*, 222, 8, doi: 10.3847/0067-0049/222/1/8
- Feroz, F., Hobson, M. P., Cameron, E., & Pettitt, A. N. 2019, *The Open Journal of Astrophysics*, 2, 10, doi: 10.21105/astro.1306.2144
- Gagné, J., Faherty, J. K., & Popinchalk, M. 2020, *Research Notes of the American Astronomical Society*, 4, 92, doi: 10.3847/2515-5172/ab9e79
- Gagné, J., Mamajek, E. E., Malo, L., et al. 2018, *ApJ*, 856, 23, doi: 10.3847/1538-4357/aaae09
- Gaia Collaboration, Brown, A. G. A., Vallenari, A., et al. 2018, *A&A*, 616, A1, doi: 10.1051/0004-6361/201833051
- Hamuy, M., Suntzeff, N. B., Heathcote, S. R., et al. 1994, *PASP*, 106, 566, doi: 10.1086/133417
- Hartman, J. D., Bakos, G. Á., Noyes, R. W., et al. 2011, *AJ*, 141, 166, doi: 10.1088/0004-6256/141/5/166
- Johnson, D. R. H., & Soderblom, D. R. 1987, *AJ*, 93, 864, doi: 10.1086/114370
- Kounkel, M., & Covey, K. 2019, *AJ*, 158, 122, doi: 10.3847/1538-3881/ab339a
- Kounkel, M., Covey, K., & G., S. K. 2020, arXiv e-prints. <https://arxiv.org/abs/2004.07261>
- Lightkurve Collaboration, Cardoso, J. V. d. M., Hedges, C., et al. 2018, *Lightkurve: Kepler and TESS time series analysis in Python, Astrophysics Source Code Library*. <http://ascl.net/1812.013>
- Luhman, K.-L., Stauffer, J.-R., & Mamajek, E.-E. 2005, *ApJ*, 628, L69, doi: 10.1086/432617
- M., H., T.-J., D., G.-D., M., & R., H. 2019, *AJ*, 158, 143, doi: 10.3847/1538-3881/ab3984
- Mamajek, E. E. 2008, *Astronomische Nachrichten*, 329, 10, doi: 10.1002/asna.200710827
- Mason, B. D., Wycoff, G. L., Hartkopf, W. I., Douglass, G. G., & Worley, C. E. 2001, *AJ*, 122, 3466, doi: 10.1086/323920
- Messina, S., Desidera, S., Turatto, M., Lanzafame, A. C., & Guinan, E. F. 2010, *A&A*, 520, A15, doi: 10.1051/0004-6361/200913644
- Metcalfe, T. S. 1999, *AJ*, 117, 2503, doi: 10.1086/300833
- Munari, U., Sordo, R., Castelli, F., & Zwitter, T. 2005, *A&A*, 442, 1127, doi: 10.1051/0004-6361:20042490
- Oelkers, R. J., & Stassun, K. G. 2018, *AJ*, 156, 132, doi: 10.3847/1538-3881/aad68e
- Oh, S., Price-Whelan, A.-M., Hogg, D.-W., Morton, T.-D., & Spergel, D.-N. 2017, *AJ*, 153, 257, doi: 10.3847/1538-3881/aa6fffd
- Penev, K., Bakos, G. Á., Bayliss, D., et al. 2013, *AJ*, 145, 5, doi: 10.1088/0004-6256/145/1/5
- Pepper, J., Kuhn, R. B., Siverd, R., James, D., & Stassun, K. 2012, *PASP*, 124, 230, doi: 10.1086/665044

- Pepper, J., Stanek, K. Z., Pogge, R. W., et al. 2008, *AJ*, 135, 907, doi: 10.1088/0004-6256/135/3/907
- Pepper, J., Pogge, R. W., DePoy, D. L., et al. 2007, *PASP*, 119, 923, doi: 10.1086/521836
- Prsa, A., Matijevic, G., Latkovic, O., Vilardell, F., & Wils, P. 2011, PHOEBE: PHysics Of Eclipsing BinariEs. <http://ascl.net/1106.002>
- Prša, A., Conroy, K. E., Horvat, M., et al. 2016, *ApJS*, 227, 29, doi: 10.3847/1538-4365/227/2/29
- Sestito, P., & Randich, S. 2005, *A&A*, 442, 615, doi: 10.1051/0004-6361:20053482
- Siverd, R. J., Beatty, T. G., Pepper, J., et al. 2012, *ApJ*, 761, 123, doi: 10.1088/0004-637X/761/2/123
- Soderblom, D. R., Jones, B. F., Balachandran, S., et al. 1993, *AJ*, 106, 1059, doi: 10.1086/116704
- Stassun, K. G., Mathieu, R. D., Vaz, L. P. R., Stroud, N., & Vrba, F. J. 2004, *ApJS*, 151, 357, doi: 10.1086/382353
- Stassun, K. G., Oelkers, R. J., Paegert, M., et al. 2019, *AJ*, 158, 138, doi: 10.3847/1538-3881/ab3467
- Stauffer, J., Barrado, D., David, T., et al. 2020, *AJ*, 160, 30, doi: 10.3847/1538-3881/ab93c9
- Stetson, P. B. 1987, *PASP*, 99, 191, doi: 10.1086/131977
- . 1990, *PASP*, 102, 932, doi: 10.1086/132719
- Tokovinin, A., Thomas, S., Sterzik, M., & Udry, S. 2006, *A&A*, 450, 681, doi: 10.1051/0004-6361:20054427
- Torres, C. A. O., Quast, G. R., da Silva, L., et al. 2006, *A&A*, 460, 695, doi: 10.1051/0004-6361:20065602
- Torres, G., Clausen, J. V., Bruntt, H., et al. 2012, *A&A*, 537, A117, doi: 10.1051/0004-6361/201117795
- Wilson, R. E., & Devinney, E. J. 1971, *ApJ*, 166, 605, doi: 10.1086/150986
- Wright, N.-J., Drake, J.-J., Mamajek, E.-E., & Henry, G.-W. 2011, *ApJ*, 743, 48, doi: 10.1088/0004-637x/743/1/48
- Yi, S., Demarque, P., Kim, Y.-C., et al. 2001, *ApJS*, 136, 417, doi: 10.1086/321795
- Zhou, G., Bayliss, D., Penev, K., et al. 2014, *AJ*, 147, 144, doi: 10.1088/0004-6256/147/6/144